mixing in the FTIR spectra made the mode assignment particularly difficult. Table III contains the results of the geometry optimizations, while Table IV gives the harmonic vibrational analysis.

Again, the most stable geometry among the several options explored was the ring structure proposed by Lascola and Andrews where both HF monomers link to form the seven-member ring sequence -F'-H'-N-O-H-F''-H''-. The MBPT(2)/6-31G* geometry is given in Figure 2. The distance between the second fluorine and the hydroxyl hydrogen is now much shorter, giving three strong hydrogen bonds versus one strong and one weak bond in the 1:1 complex. As a result, the association enthalpy of the 1:2 complex is almost 3 times larger as documented in Table VI. These results give an association enthalpy of about -17 to -19 kcal/mol at the MBPT(2) or SDQ-MBPT(4) levels for this complex. With use of the MBPT(2)/6-31G* results, the N-HF and F-HO distances in the 1:2 complex have values of 1.57 and 1.78 Å, which are appreciably shorter than those of 1.71 and 2.01 Å in the 1:1 complex. Additionally, the HF-HF bond distance in the 1:2 complex is only 1.56 Å, much shorter than that of 1.68 Å found in the dimer $(HF)_2$ at the MBPT(2)/6-31G* level. The ring structure is much tighter than expected.

As observed by Lascola and Andrews, the vibrational mode mixing was considerable, making the assignments of the modes in Table IV very crude at best except for the higher frequency modes. Due to computing constraints, the vibrational analysis of the trimer was completed at the SCF/6-31G* level of theory rather than the MBPT(2)/6-31G** level used for the dimer. However, as the data in Table IV indicate, the two levels gave similar results for the dimer. Only twice, when there was significant mode mixing, were two frequencies interchanged. The intensities compared favorably, and both methods gave the same signs for the perturbations to the frequencies of the monomers, i.e., ω(dimer) - ω(monomer). For the trimer, the qualitative perturbations to the vibrational modes, as elaborated in Table VIII, were what would be expected from the effects of hydrogen bonding.

Conclusions

These results substantiate many of the conclusions derived from the FTIR spectra of the $(HF)_nH_2NOH$ clusters. The 1:2 complex however exhibited tighter than expected bonding. For the 1:1 and 1:2 complexes, the association energies are approximately -6 to -9 and -17 to -19 kcal/mol, respectively. Most of the assumptions made in the vibrational assignments for the 1:1 complex appear to be valid.

Acknowledgment. R.J.B. thanks the U.S. Office of Naval Research, and R.E.B. thanks the National Science Foundation and the NSF Supercomputer Center at Pittsburgh. These computations were made under their grant (NSF/PSC Grant No. CHE870047P).

Registry No. HF, 7664-39-3; H_2NOH, 7803-49-8.

A Copper(II) Bromide Dimer System Exhibiting Piezochromic and Thermochromic Properties: The Crystal Structure and Electronic Spectroscopy of the Two Room-Temperature Phases of Bis(tetrapropylammonium) Hexabromodicuprate(II)

Brian Scott and Roger D. Willett*

Contribution from the Department of Chemistry, Washington State University, Pullman, Washington 99164-4630. *Received October 9, 1990*

Abstract: Two phases of the compound bis(tetrapropylammonium) hexabromodicuprate(II) were synthesized and their crystal structures determined. The orange phase exhibits piezochromism, with the application of a small force causing it to spontaneously transform to the green phase. The green phase is thermochromic and transforms to the orange phase upon heating to 90 °C. The green triclinic phase, with space group $P\bar{1}$, a = 9.612 (2) Å, b = 9.602 (2) Å, c = 12.006 (3) Å, α = 102.27 (2)°, β = 104.30 (2)°, γ = 112.79 (1)°, V = 929.2 (3) Å^3, Z = 1, d_x = 1.75 g/cm^3, and R = 0.0642, is stable at room temperature. The orange phase, metastable at room temperature, is monoclinic with space group $C2/c$, a = 17.460 (6) Å, b = 14.625 (4) Å, c = 15.061 (4) Å, β = 103.82 (2)°, V = 3735 (2) Å^3, Z = 4, d_x = 1.74 g/cm^3, and R = 0.0839. Both phases have isolated $Cu_2Br_6^{2-}$ dimers with very similar geometries. The correlation of polarized absorption spectral data and X-ray crystallography show that the difference in orientation of the $Cu_2Br_6^{2-}$ chromophores in the two phases is responsible for the color variance. A prominent feature of the visible absorption spectra is the presence of a so-called "dimer" transition at approximately 13 000 cm^{-1}. This assignment gives strong support for ligand to metal character of the dimer transition, and not a simultaneous excitation of d-d transitions on both copper centers. EHMO calculations support this assignment.

Introduction

The compound to be described in this work has many interesting features. First, it is a thermochromic compound in which high- and low-temperature phases coexist at room temperature. This is not itself unknown,[1] but the fact that the high-temperature phase is metastable—a small stress to the crystal causes it to spontaneously transform to the low-temperature phase—is unusual. Second, the color difference between the two phases is not the result of a change in coordination geometry or ligand field strength, as is commonly observed in copper halide materials. The majority of these materials consist of networks of $CuCl_4^{2-}$ anions linked to ammonium groups on the cations via hydrogen bonding. The change in coordination geometry, from square planar to tetrahedral, is caused by weakening of this hydrogen-bonding network, brought on by increased thermal motion in the cations as the temperature is raised.[2] In the only thermochromic dimer systems, $[(CH_3)_2CHNH_3]_2Cu_2X_6$ with X = Cl or Br, a striking change

(1) Battaglia, L. P.; Bonamartini-Corradi, A.; Marcotrigiano, G.; Menabue, L.; Pellacani, G. C. *Inorg. Chem.* **1982**, *21*, 3919.

(2) Bloomquist, D. R.; Willett, R. D. *Coord. Chem. Rev.* **1982**, *47*, 125.

0002-7863/91/1513-5253$02.50/0

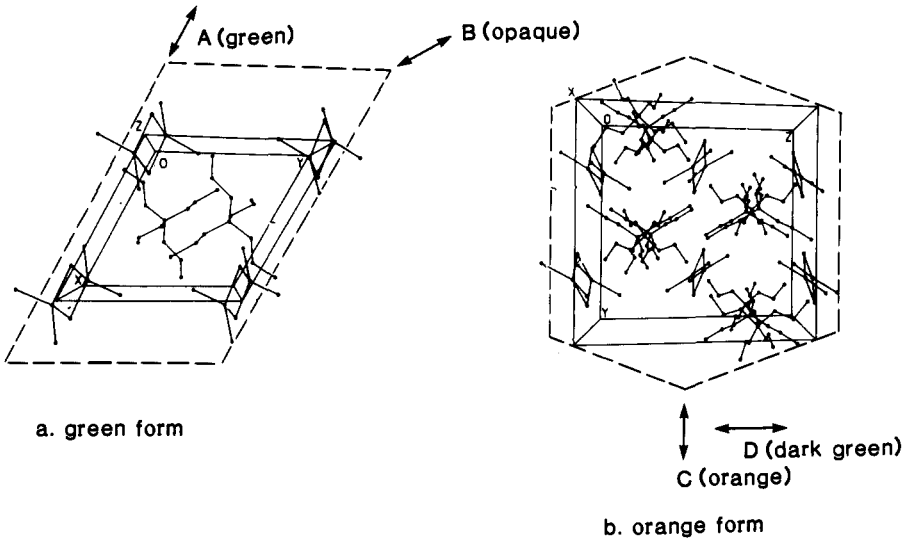

Figure 1. Unit cell packing diagram of the green (a) and orange (b) forms of $(TPA)_2Cu_2Br_6$. The dashed lines show the crystal morphology. The arrows show polarization directions for the polarized absorption experiment.

in coordination geometry takes place: from stacked dimeric units to infinite tribridged copper halide chains.[3] This transformation is also brought on by a change in hydrogen bonding resulting from increased thermal motion of the isopropylammonium cation. In contrast, the title compound consists of $Cu_2Br_6^{2-}$ dimers isolated from each other by tetrapropylammonium cations, and thus no hydrogen-bonding network exists. The mechanism for color change is a shift in the orientation of the $Cu_2Br_6^{2-}$ anions. In this paper, polarized spectra, crystal structures, and EHMO calculations will be used to argue this orientation mechanism. Last, the origin of the dimer band, a source of controversy in years past,[4] will be shown to arise from a ligand to metal charge-transfer transition and not a simultaneous pair excitation. Absorption spectra and EHMO calculations will be used to show that this transition arises from a new ligand-based molecular orbital created upon dimer formation, and not the result of two simultaneous CuX_4^{2-} ligand field transitions.

Experimental Section

Synthesis. Both phases of the title compound were made by dissolving, with heat, stoichiometric amounts of $CuBr_2$ and tetrapropylammonium bromide in a 1:4 concentrated HBr–ethyl acetate solution. This solution was then allowed to cool slowly, and within 1 h orange elongated hexagonal-shaped plates and green diamond-shaped plates had crystallized. The color classification is based on the crystals color when viewed with white light transmitted perpendicular to the flat face of the platelet. Both forms are highly pleochroic and may be forced to have similar colors if each is held in the proper orientation. The orange form may be converted to the green form by applying a small stress to the crystal. This transformation manifests itself as a green wave moving across the face of the crystal, taking 1–2 s to traverse a crystal 0.5 mm wide. The wavefront travels in the (001) direction (Figure 1). The hexagonal-shaped orange plates often fracture into smaller diamond-shaped green plates as the transformation occurs. The green form transforms to the orange form when heated to 90 °C.

X-ray. A crystal of the green form with dimensions 0.05 × 0.11 × 0.18 mm and a crystal of the orange form with dimensions 0.07 × 0.21 × 0.45 mm were mounted on thin glass fibers. Great care was taken not to shock the orange form, and the crystal was optically checked after data collection to assure phase homogeneity. Data sets on both forms were collected on a Syntex $P2_1$ (upgraded to Nicolet R3 specifications) with graphite-monochromatized Mo Kα (λ = 0.71069 Å) radiation.[5] The lattice constants for the orange and green forms were optimized from the least-squares refinement to the angular settings of 25 carefully centered Bragg reflections in the ranges $16° < 2\theta < 19°$ and $24° < 2\theta < 30°$, respectively. Figure 1 shows the indexing of crystal faces for both forms. The SHELXTL 5.1 software package was used for data reduction and refinement.[6] A summary of crystal parameters is listed in Table I, with atomic positions and isotropic thermal parameters deposited as supplementary material.

Table I. Crystallographic Data for $[(C_3H_7)_4]_2Cu_2Br_6$

	green form	orange form
a, Å	9.612 (2)	17.460 (6)
b, Å	9.602 (2)	14.625 (4)
c, Å	12.006 (3)	15.061 (4)
α, deg	102.27 (2)	90.0
β, deg	104.30 (2)	103.82 (2)
γ, deg	112.79 (1)	90.0
V, Å^3	929.2 (3)	3735 (2)
Z	1	4
formula weight	979.22	979.22
space group	$P\bar{1}$ (No. 2)	$C2/c$ (No. 15)
T, °C	22	22
λ, Å	0.71069	0.71069
ρ_{calc}, g/cm^3	1.75	1.74
μ, cm^{-1}	75.6	75.2 cm^{-1}
transmission coeff	0.59–0.96	0.53–0.97
$R(F_o)$	0.0642 (0.097, all reflxn)	0.0839 (0.1355, all reflxn)
$R_w(F_o)$	0.0552 (0.0605, all refxn)	0.0781 (0.0897, all reflxn)

Powder Diffraction. Powder diffraction patterns of virgin crystalline samples of the orange and green phases, and of the orange and green phases obtained from phase transformations, were taken on a Siemans D500 powder diffractometer using Co Kα (λ = 1.7902 Å) radiation. In addition, powder patterns simulated from the single-crystal coordinates were generated by the XFIT program from SHELXTL version 5.1.

Optical Properties. When viewed with polarized light, the two crystalline forms exhibit the following behavior:

Green form: Viewed with polarized light perpendicular to the (001) face, crystals appear green when the direction of polarization is parallel to (100) (labeled A in Figure 1a) and are opaque when the polarization direction is parallel to the (110) direction. When a green crystal is tipped on edge, so that the light is traveling perpendicular to the (010) face, the following is observed: The crystal appears orange when the light is polarized parallel to (100) and green with the light polarized parallel to (010).

Orange form: With light perpendicular to the (100) face, crystals appear orange when the light is polarized parallel to the (010) direction (labeled C in Figure 1b) but green when polarized parallel to the (001) direction (labeled D in Figure 1b). When viewed on edge, the crystal appears opaque when the light is polarized parallel to (001) and green when polarized parallel to (010).

(3) Roberts, S. A.; Bloomquist, D. R.; Willett, R. D.; Dodgen, H. W. *J. Am. Chem. Soc.* **1981**, *103*, 2603.

(4) (a) Hansen, A. E.; Ballhausen, C. J. *Trans. Faraday Soc.* **1965**, *61*, 631. (b) Dubicki, L. *Aust. J. Chem.* **1972**, *25*, 1141. (c) Desjardins, S. R.; Wilcox, D. E.; Musselman, R. L.; Solomon, E. I. *Inorg. Chem.* **1987**, *26*, 288.

(5) Campana, C. F.; Shepard, D. F.; Litchman, W. M. *Inorg. Chem.* **1981**, *20*, 4039.

(6) Sheldrick, G. SHELXTL, Version 5.1, Nicolet Analytical Instruments, Madison, WI, 1985.

Ligand Field Spectra. The single-crystal near-IR (6000–12 000-cm^{-1}) absorption spectra on both phases were taken on a Perkin-Elmer 1700X series FTIR. The standard Perkin-Elmer condensing attachment for single-crystal work was used. The light was incident upon the *ab* face in the green form and the *bc* face in the orange form (Figure 1).

Charge-Transfer Spectra. All of the single-crystal-polarized absorption spectra in the visible region (11 630–25 000 cm^{-1}) were taken on a Perkin-Elmer 330, fitted with condensing optics and employing sheets of polaroid film to polarize the source. The crystals were mounted over pinholes in aluminum foil. The radiation was polarized as shown in Figure 1. This polarization scheme eliminates the possibility of elliptical polarization in the orange monoclinic form.[4c]

EHMO Calculations. The program EHT[7] was used for the calculation. The coordinates of bis(tetraphenylarsonium) hexachlorodicuprate(II) were used in the calculation for reasons discussed below.[8] The geometry of the $Cu_2Cl_6^{2-}$ dimer in this compound is very similar to those of the $Cu_2Br_6^{2-}$ dimers of the title compound. Small adjustments were made in the dimer coordinates in order to achieve perfect C_{2h} symmetry. The bridging Cu–Cl bond distances were fixed at 2.29 Å and the terminal Cu–Cl bond distances at 2.19 Å. The *x* axis of the coordinate system was placed along the Cu–Cu 2-fold axis of the dimer, and the *y* axis was placed so that the *xy* plane was perpendicular to the local S_4 axis of the D_{2d} $CuCl_4$ coordination sphere. The orbital exponents for the s and p orbitals (single ζ) on the Cu and Cl atoms, the orbital exponents and coefficients for the Cu 3d orbitals (double ζ), and the valence scale ionization potentials for all atoms were taken from a previous publication by Hoffmann on $Cu_2Cl_6^{2-}$ dimer systems.[9] The basis orbitals for Cl were used since the EHT program does not accommodate different values for s- and p-orbital exponents on the bromine atoms. This does not present a problem, since the goal of the calculation is not to calculate the magnitude of the energy levels but rather to gain a qualitative feeling for their ordering and composition, from which the nature of the electronic transitions may be ascertained.

Results and Analysis

Structure Description. The crystal structures of both phases contain $Cu_2Br_6^{2-}$ dimers located on centers of inversion and isolated by tetrapropylammonium cations. The geometry at each copper(II) center is nearly D_{2d}, with a geometry intermediate between tetrahedral and square planar. The bond distances of 2.340 (1)/2.346 (3) Å and 2.333 (1)/2.330 (3) Å for terminal Cu–Br bonds in the green/orange forms are considerably shorter than the bridging bond distances of 2.441 (3)/2.448 (2) Å and 2.417 (3)/2.440 (2) Å for the green/orange forms. The average trans angles, which characterize the D_{2d} distortion of the coordination geometry, are 146.4 (1)° and 148.1 (1)° for the green and orange forms respectively. The other Br–Cu–Br bond angles range from 86.7 (1)° to 99.1 (1)° and 87.2 (1)° to 97.8 (1)° for the green and orange forms, respectively. The bridging Cu–Br–Cu angle for the green form is 93.3 (1)° and 92.8 (1)° for the orange form. The geometries about the copper(II) centers in these salts place them in the structural class of isolated, twisted dimers.[10] These dimers occur is systems with large, bulky non-hydrogen-bonding counterions. They are structurally characterized by the twist angle, τ, which is the dihedral angle between the bridging Cu_2X_2 plane and the terminal CuX_2 plane. In the green form $\tau = 46.4°$, and in the orange form $\tau = 44.2°$. In comparison, the twist angles for $(Ph_4As)Cu_2Cl_6$ and $(Ph_4P)Cu_2Cl_6$ are approximately 50°, with about the same values for the bromide analogues. The twist angle ranges from 44° to 85° for known twisted dimers. In the orange form the cations are sitting on sites of 2-fold symmetry, while in the green form the cations are sitting in general positions. In both instances, the propyl groups assume an all-trans conformation. The major difference between the cations in the two phases is thermal motion of the propyl groups; the average isotropic *U* for the carbon atoms of the propyl groups is 0.180 $Å^2$ for the orange form and 0.070 $Å^2$ for the green form. In contrast, the average isotropic *U* for the Cu and Br atoms in the orange form is only 30% greater than that of the green form. A view of the $Cu_2Br_6^{2-}$ dimers of both forms showing thermal ellipsoids and bond distances and angles is shown in Figure 2.

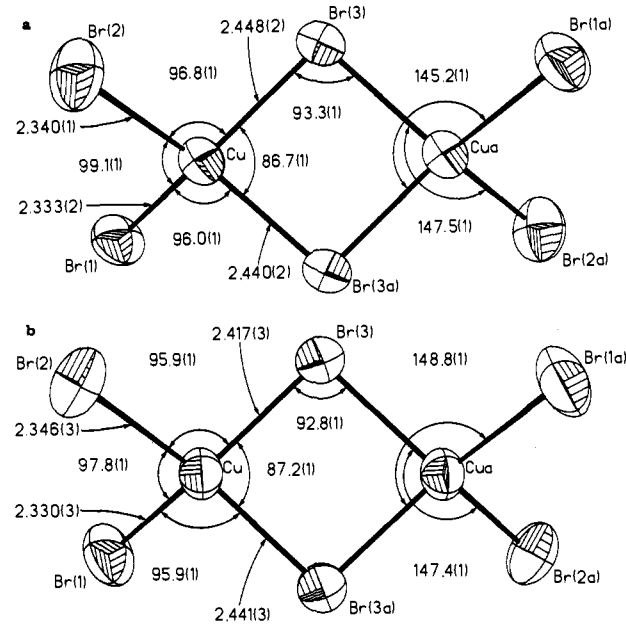

Figure 2. Diagram showing the $Cu_2Br_6^{2-}$ dimer portions of the (a) green and (b) orange forms.

The major structural difference between the two phases is the orientation of the above, almost identical dimers within the unit cell of each phase. The unit cell packing diagrams are shown in Figure 1. The high-temperature orange monoclinic phase has two slightly different orientations of the dimer in the unit cell, while the room-temperature green triclinic phase has only one. The copper–copper axis of the dimer is almost perpendicular to the (100) face of the orange platelets; however, a small component does lie parallel to the *c* axis in the *bc* plane. A substantial component of the Cu–Cu vector lies parallel to the (001) face of the platelet in the green form (Figure 3), with the projection onto this plane nearly parallel to the (110) direction.

Powder Diffraction Results. The powder diffraction pattern of the virgin room-temperature green form agreed very well with the pattern generated from the single-crystal coordinates of the green form. The powder pattern of the orange form obtained from heating of the green form agreed very well with the pattern generated from single-crystal coordinates of the orange form. The powder pattern of the green form obtained from grinding of the orange form, which was obtained by heating the green form obtained from solution, showed a superposition of the orange and green patterns generated from the single-crystal coordinates, but no new peaks were observed. The powder patterns give direct evidence of the presence of only two phases; the orange and green phases obtained from solution and the corresponding orange and green phases obtained from phase transformations are identical phases.

EHMO Calculations. The extended Huckel results show the typical bonding picture for a transition-metal complex: an antibonding block of orbitals which are primarily Cu 3d in composition, with a bonding block of orbitals showing large chlorine 3p character lying lower in energy. The two molecular orbitals at the top of the d block, of b_{1u} and b_{1g} symmetry, have two electrons distributed between them and are close in energy (about 2000 cm^{-1} apart). The exact composition of these orbitals is shown in Table II. Also shown are the compositions of the top four ligand orbitals, which are of b_{1u}, b_{1g}, a_{1u}, and a_{1g} symmetry. In analogy to the planar parent $Cu_2X_6^{2-}$ species of D_{2h} symmetry, the upper two partially occupied orbitals are symmetric and antisymmetric combinations of $d_{x^2-y^2}$-like orbitals lying in the least-squares plane of the halogen atoms, with strong antibonding contributions from the p orbitals on the bridging halogen atoms.

(7) Quantum Chemistry Program Exchange, Chemistry Department, Room 204, Indiana University, Bloomington, IN 47401.
(8) Scott, B.; Willett, R. D. *Acta Crystallogr. C* **1991**, *47*, 435.
(9) Hay, P. J.; Thibeault, J. C.; Hoffmann, R. *J. Am. Chem. Soc.* **1975**, *97*, 4884.
(10) Willett, R. D.; Grigereit, T.; Halvorson, K.; Scott, B. *Proc. Indian Acad. Sci. (Chem. Sci.)* **1987**, *98* (1 & 2), 147.

Table II. Coefficients and Energies of Selected Molecular Orbitals for the Twisted $Cu_2Cl_6^{2-}$ Dimer Obtained from EHMO Calculations (Atom Labels Correspond to the Bromine and Copper Labels in Figure 2)

	metal orbitals		chlorine pπ(nonbonding) orbitals			
AO	b_{1u}(Cu)	b_{1g}(Cu)	b_{1u}(Cl)	b_{1g}(Cl)	a_{1u}(Cl)	a_{1g}(Cl)
energy/eV	−12.161	−12.434	−15.271	−15.315	−15.396	−15.416
s(Cl1)	0.055	0.053	−0.003	−0.002	0.000	0.003
s(Cl2)	−0.055	−0.053	0.003	0.002	0.000	0.003
s(Cl3)	0.116	0.000	0.005	0.000	0.033	0.000
s(Cl1a)	−0.055	0.053	0.003	−0.002	0.000	−0.003
s(Cl2a)	0.055	−0.053	−0.003	0.002	0.000	−0.003
s(Cl3a)	−0.116	0.000	−0.005	0.000	−0.033	0.000
s(Cu)	0.000	0.000	0.000	0.000	0.000	−0.037
s(Cua)	0.000	0.000	0.000	0.000	0.000	0.037
p_x(Cl1)	0.011	0.115	0.211	0.323	0.251	0.220
p_x(Cl2)	−0.011	−0.115	−0.211	−0.323	−0.251	0.220
p_x(Cl3)	0.000	−0.312	0.000	−0.198	0.001	0.337
p_x(Cl1a)	0.011	−0.115	−0.211	−0.323	0.251	0.220
p_x(Cl2a)	−0.011	0.115	−0.211	0.323	−0.250	0.220
p_x(Cl3a)	0.000	0.312	0.000	0.198	0.001	0.337
p_x(Cu)	0.000	0.000	0.000	0.000	0.000	−0.048
p_x(Cua)	0.000	0.000	0.000	0.000	0.000	0.048
p_y(Cl1)	0.137	0.138	−0.293	−0.321	−0.167	−0.096
p_y(Cl2)	0.137	0.138	−0.293	−0.321	−0.167	0.096
p_y(Cl3)	−0.231	0.000	−0.217	0.000	0.485	−0.002
p_y(Cl1a)	0.137	−0.138	−0.293	0.321	−0.167	−0.096
p_y(Cl2a)	0.137	−0.138	−0.293	0.321	−0.167	0.096
p_y(Cl3a)	−0.231	0.000	−0.217	0.000	0.485	0.002
p_y(Cu)	−0.005	−0.039	0.036	0.016	−0.036	0.000
p_y(Cua)	−0.005	0.039	0.036	−0.016	−0.036	0.000
p_z(Cl1)	0.106	0.116	−0.198	−0.136	0.153	0.335
p_z(Cl2)	0.106	0.116	−0.198	−0.136	0.153	−0.335
p_z(Cl3)	0.205	0.000	0.328	0.000	−0.033	−0.001
p_z(Cl1a)	0.106	−0.116	−0.198	0.136	0.153	0.335
p_z(Cl2a)	0.106	−0.116	−0.198	0.136	0.153	−0.335
p_z(Cl3a)	0.205	0.000	0.328	0.000	−0.033	0.001
p_z(Cu)	−0.099	−0.090	−0.001	−0.014	0.017	0.000
p_z(Cua)	−0.099	0.090	−0.001	0.014	0.017	0.000
d_{z^2}(Cu)	0.000	0.000	0.000	0.000	0.000	−0.082
d_{z^2}(Cua)	0.000	0.000	0.000	0.000	0.000	0.082
d_{xz}(Cu)	0.015	−0.002	−0.090	−0.120	0.120	0.000
d_{xz}(Cua)	−0.015	−0.002	0.090	−0.120	−0.120	0.000
d_{yz}(Cu)	0.000	0.000	0.000	0.000	0.000	0.135
d_{yz}(Cua)	0.000	0.000	0.000	0.000	0.000	−0.135
d_{xy}(Cu)	−0.617	−0.610	0.054	0.028	−0.112	0.000
d_{xy}(Cua)	0.617	−0.610	−0.054	0.028	0.112	0.000
$d_{x^2-y^2}$(Cu)	0.000	0.000	0.000	0.000	0.000	−0.092
$d_{x^2-y^2}$(Cua)	0.000	0.000	0.000	0.000	0.000	0.092

Table III. Summary of Copper(II) Halide Transition Energies (cm^{-1})

transition	$(TBA)_2CuBr_4$[a]	$(TBA)_2Cu_2Br_6$[a]	$(TPA)_2Cu_2Br_6$[c]	(cin)$CuCl_4$[b]	$(Ph_4As)_2Cu_2Cl_6$[a]
d–d	8300 (br)	6700/11 100	9250/11 000	9100/11 100	11 100/8500
dimer		not measd	13 070		21 700
π(nb) → $d_{x^2-y^2}$	16 600	15 400	15 870	26 000/22 500[d]	24 600
π(b) → $d_{x^2-y^2}$	19 000	19 300	20 410/19 230[d]	34 780/32 200[d]	31 900

[a] Reference 15. TBA is tetrabutylammonium. [b] Reference 20. This compound is bis[(cinchonium) tetrachlorocuprate(II)] trihydrate, with a trans angle of 145°. [c] This work. [d] Shoulder.

This pair of orbitals become closer in energy as the dimer geometry goes from planar to twisted since the p_x orbitals on the bridging halides are no longer oriented favorably for effective overlap with the d orbitals in the b_{1g} orbital. These orbitals cross at a twist angle of 35°, and ferromagnetic coupling is observed.[9] The top four ligand-based orbitals are essentially nonbonding in nature, and involve largely ligand p(π)-type orbitals. A small, but significant, increase in bonding Cu d-orbital contribution occurs with decreasing orbital energy for these four orbitals.

Ligand Field Spectra. The ligand field spectra for both forms are shown in Figure 3. The spectrum for the green form clearly shows two broad peaks centered at approximately 11 000 and 9250 cm^{-1}. The spectrum for the orange form shows a broad peak at about 10 750 cm^{-1}, with a broad shoulder at approximately 9250 cm^{-1}. The difference in intensity between the bands at 9250 cm^{-1} in the two spectra is attributed to a polarization effect.

To assign the above portion of the $(TPA)_2Cu_2Br_6$ spectra, an appeal is made to the interpretation of the spectra of copper(II) chloride species containing tetrahedrally distorted $CuCl_4$ coordination spheres. The ligand field strength of the Br^- anion is approximately equal to that of the Cl^- anion. Thus, the ligand field bands, for a given geometry, should occur at the same energies. In addition, the ligand field spectrum of the $Cu_2Cl_6^{2-}$ dimer has been assigned very well in terms of the D_{2d} $CuCl_4^{2-}$ monomer.[4c] The success of this method is a result of the approximate D_{2d} geometry about the Cu atom in the dimer systems and the fact that the monomer energies of the d orbitals are not significantly changed upon dimer formation.[11,12] A comparison of transition energies for several copper(II) halide species is shown in Table III, and an energy level diagram for a D_{2d} $CuCl_4^{2-}$ monomer is shown in Figure 4. (This energy level diagram was drawn on the basis of several previous works.[4,22] Four types of transitions are predicted: (1) ligand field transitions from the e, b_1, and a_1

(11) Willett, R. D.; Liles, O. L., Jr. *Inorg. Chem.* **1967**, *6*, 1666.
(12) Smith, D. W. *Coord. Chem. Rev.* **1976**, *21*, 93.

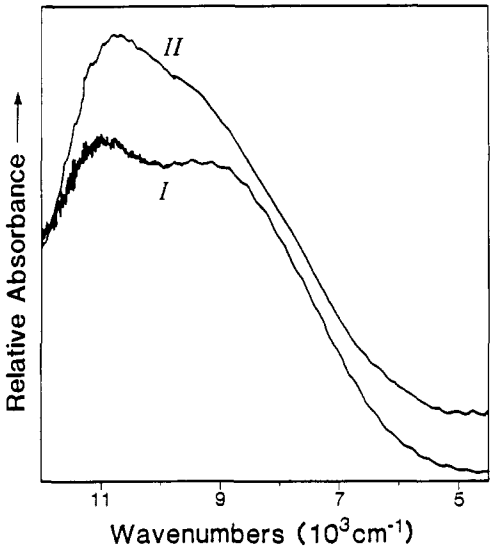

Figure 3. d–d single-crystal spectrum of both forms: I, green form; II, orange form. These spectra were taken with ordinary light incident upon the *ab* face in the green form and the *bc* face in the orange form (Figure 1).

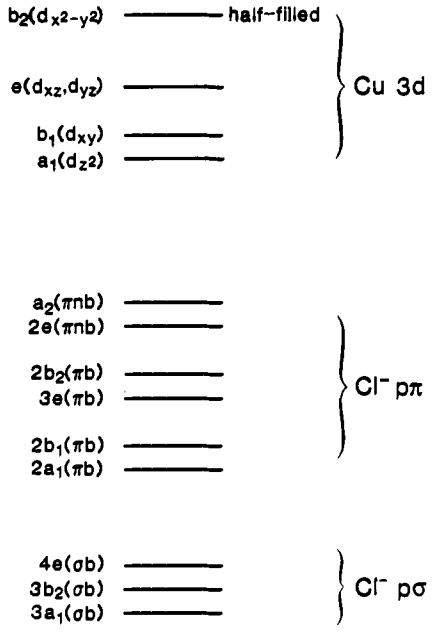

Figure 4. Energy level diagram of the D_{2d} $CuCl_4^{2-}$ ion.

orbitals of the d block to the half-filled $b_2(d_{x^2-y^2})$ orbital, (2) ligand p_π(nonbonding) to the metal $b_2(d_{x^2-y^2})$ orbital, (3) ligand p_π(bonding) to the metal $b_2(d_{x^2-y^2})$ orbital, (4) ligand p_σ(bonding) to the metal $b_2(d_{x^2-y^2})$ orbital. Transitions 2 and 3 will be used to assign the charge-transfer transitions in the following section. The assignments in Table III correspond to these transitions.)

The majority of D_{2d} monomer complexes[12] show two broad d–d bands, the higher energy being assigned to the $^2B_2 \rightarrow {}^2A_1$ ($d_{z^2} \rightarrow d_{x^2-y^2}$) and $^2B_2 \rightarrow {}^2B_1$ ($d_{xy} \rightarrow d_{x^2-y^2}$) transitions and the lower energy band being assigned to the $^2B_2 \rightarrow {}^2E$ ($d_{xz},d_{yz} \rightarrow d_{x^2-y^2}$) transition (Figure 4). The energy of these transitions has been shown to be directly proportional to the $CuCl_4^{2-}$ trans angle.[13] For complexes with trans angles from 120° to 140°, the two bands occur in the range of 9000–11000 and 6000–9000 cm^{-1}, respectively. The dimer complexes $(Ph_4As)_2Cu_2Cl_6$ and $(Ph_4P)_2Cu_2Cl_6$ have average trans angles of 143.4° and 144.8°, respectively.[8,14] The

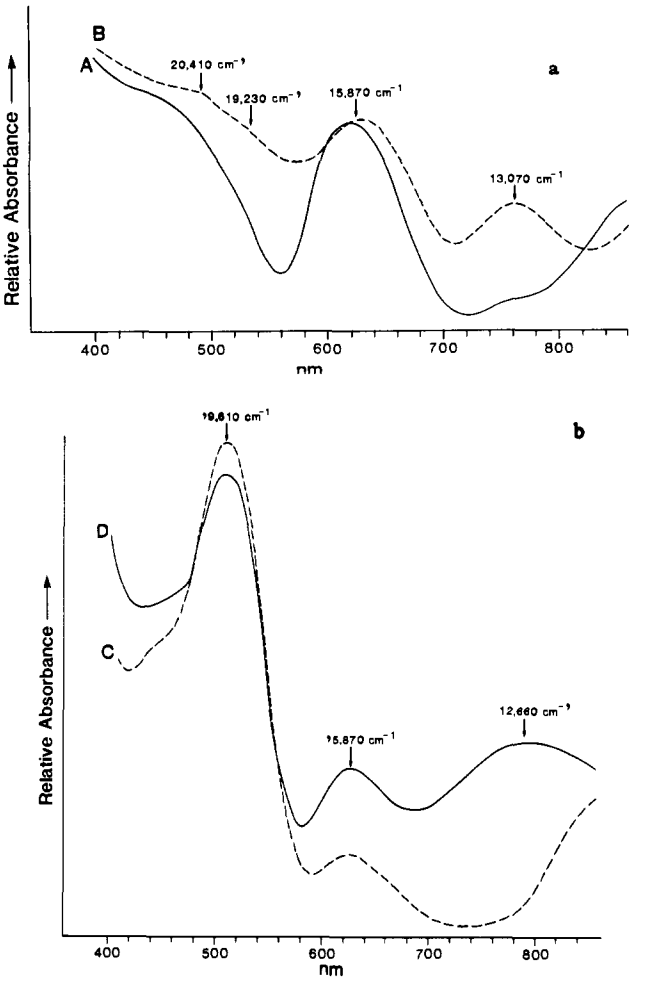

Figure 5. Polarized absorption spectra for the green (a) and orange (b) forms. The capital letters refer to the polarization directions shown in Figure 1.

ligand field spectra for these dimers[15] both show broad peaks around 11 000 and 8250 cm^{-1} (Table III). It is thus reasonable to assume that the observed transitions of the title compound at 9250 and 11 000 cm^{-1} correspond to the above broad D_{2d} transitions.

Charge-Transfer Spectra. The single-crystal-polarized spectra for both forms are shown in Figure 5. Spectra A and B were taken on the green form, and spectra C and D were taken on the orange form. The letters refer to the polarization directions shown in Figure 1. A sharp maxima at approximately 19 610 cm^{-1} is observed in spectra C and D, while in spectra A and B this region has a small bump at 20 410 cm^{-1}, with a shoulder at about 19 230 cm^{-1}. All four spectra have a broad band at approximately 15 870 cm^{-1}. In spectrum B a broad absorption occurs at 13 070 cm^{-1}, and in spectrum D an even broader absorption occurs at 12 660 cm^{-1}.

Again, assignment of the spectrum is based on analogy to the corresponding chloride systems (Table III). It has been shown in previous works[11,12] that the major difference between the $Cu_2Cl_6^{2-}$ absorption spectrum and the $CuCl_4^{2-}$ absorption spectrum is the presence of the dimer band around 19 000 cm^{-1}. It is characterized by a strong polarization along the Cu–Cu direction and has an energy intermediate between the highest energy d–d band and the lowest energy charge-transfer band of the monomer. All other bands are common to either chromophore and occur at the same energies for similar Cu environments.

In the bromide dimer, the only band polarized along the Cu–Cu axis of the dimer, and thus a candidate for the dimer transition,

(13) (a) Harlow, R. L.; Wells, W. J., III; Watt, G. W.; Simonsen, S. H. *Inorg. Chem.* **1975**, *14*, 1768. (b) McDonald, R. G.; Riley, M. J.; Hitchman, M. A. *Inorg. Chem.* **1988**, *27*, 894.

(14) Textor, M.; Dubler, E.; Oswald, H. R. *Inorg. Chem.* **1974**, *6*, 1361.
(15) Ludwig, W.; Textor, M. *Helv. Chim. Acta* **1971**, *54*, 1143.

is the one at 13 070 cm^{-1}. The energy levels obtained from the EHMO calculation are shown in Table II. The only allowed transitions polarized along the Cu–Cu axis of the dimer arise from the nonbonding b_{1u} and b_{1g} orbitals at the top of the ligand orbital block. This agrees with the position of the band at 13 070 cm^{-1}, which is the first band on the high-energy side of the ligand field transitions. Also, this band is not observed in the $CuBr_4^{2-}$ monomer (Table III). The transition at 13 070 cm^{-1} is thus assigned to the dimer transition and arises from the b_{1u}(ligand) → b_{1g}(metal) and b_{1g}(ligand) → b_{1u}(metal) transitions. The b_{1u} and b_{1g} metal orbitals are close in energy, and both singlet–singlet and triplet–triplet transitions are postulated. The broad band at 12 660 cm^{-1} in the orange form is believed to be a superposition of the dimer band, observed at 13 070 cm^{-1} in the green form, and the ligand field transition at 11 000 cm^{-1}. A polarization effect is postulated as the cause for the large role of the d–d transition in the orange form, but not in the green form. The two remaining dominant bands were assigned in analogy to the assignments for the D_{2d} point group of the $CuCl_4^{2-}$ monomer; the bands at 19 610 and 20 410 cm^{-1} are assigned to the $^2B_2 \rightarrow {}^2E(3e(\pi b) \rightarrow b_2)$ transition (Figure 4). The transition at 15 870 cm^{-1} is assigned to the $^2B_2 \rightarrow {}^2E$ $(2e(\pi nb) \rightarrow b_2)$ transition (Figure 4). The band at 19 230 cm^{-1}, a shoulder on the band at 20 410 cm^{-1}, is assigned to the $^2B_2 \rightarrow {}^2B_2(2b_2(\pi b) \rightarrow b_2)$. A shoulder on the band at 15 870 cm^{-1}, which would be assigned to the $^2B_2 \rightarrow {}^2A_2$ $(a_2(\pi nb) \rightarrow b_2)$ transition, was not observed.

Discussion

An examination of the spectra in Figure 5 shows several bands with strong polarization dependence. The presence of such bands accounts for the high degree of pleochromism within each phase of the title compound. The color of the two phases under transmitted ordinary and polarized light can be understood on the basis of these spectra. Spectrum A has "windows" in the absorption spectrum at ~14 000 and 18 000 cm^{-1}: the transmitted light thus appears green. For the B spectrum, strong absorption occurs across the whole spectrum and the sample is opaque. For unpolarized light, the only light transmitted is through the 14 000- and 18 000-cm^{-1} windows in the A spectrum. Thus, the crystals appear green. For the other phase, the C spectrum shows a window at 14 000 cm^{-1}, so the sample appears orange in this orientation. The spectrum for the orange phase is dominated in both polarizations by the strong absorption at 19 600 cm^{-1}; thus, the sample appears orange. In the D spectrum, however, the 15 870-cm^{-1} band and the dimer bands lead to significant absorption at longer wavelength. The dark green color for this orientation is associated with the "window" near 18 000 cm^{-1}. An equivalent interpretation of the origin of the crystal colors is as follows: The orange crystal is so colored due to its intense absorbance around 500 nm, while the green crystal is so colored due to its small absorbance around 500 nm (Figure 5).

It was pointed out above that the two phases can be made to have identical colors if the crystals were held in the proper orientations with respect to the light source. In essence, it is the dimer orientations that are becoming coincident. This coincidence may be achieved by simply moving the whole crystal, or leaving the crystals stationary and moving the dimers within the crystals. The latter suggestion seems absurd at first, but it turns out that this is precisely what happens during the phase transition. During the phase transformation, from orange plates to green plates, the dimers are changing their orientations from those in Figure 1b to those in Figure 1a. The color change accompanying the transition and the fragmentation of the orange hexagonal shaped plates into green diamond-shaped plates are evidence of this mechanism of transformation.

The higher symmetry and lower density of the orange phase are consistent with its stability at high temperature. In the orange monoclinic phase the tetrapropylammonium ions are located on sites of 2-fold symmetry. The increased unit cell volume for the orange phase provides more freedom for the cation and allows it to be situated at a site of higher symmetry. The fact that the carbon atoms in the propyl groups of the orange form have much larger thermal motion than in the green form is in agreement with this picture. In general, higher temperatures favor more open structures and higher pressures favor more compact structures. The existence of both phases at room temperature is a result of a fairly high energy barrier for the transformation from the orange to green phase. As the solution began crystallization, the orange form formed first. The green form, stable at lower temperatures, crystallized in a cooler solution. The orange phase coexisted in this cooler region since sufficient activation energy to overcome the energy barrier for transformation to the green form did not exist. Application of pressure to the orange form lowered the energy barrier and allowed the transformation to occur.

The entire spectrum of the $Cu_2Br_6^{2-}$ dimer makes a solid case for the ligand to metal charge-transfer assignment of the dimer band. In order for the dimer transition to be a simultaneous pair excitation (SPE), it would need to have an energy 2 times that of one of the d–d transitions. In the chloride complexes the energies of the dimer transitions are right at 2 times the energy of the d–d transitions, and thus an assignment problem arises. In the bromide, however, the energy of the dimer transition has moved to substantially lower energy, while the d–d transitions are at approximately the same energy. In Figure 3, the d–d spectrum of the green form shows peaks at 11 000 and 9200 cm^{-1}, which would put the energy of a simultaneous d–d transition at 18 400–22 000 cm^{-1}. In Figure 5a the energy of the dimer transition is observed to be approximately 13 000 cm^{-1}, and thus the SPE assignment is disproven.

Conclusions

The green triclinic form of the title compound is the stable modification below 90 °C, with the orange monoclinic form being the stable modification above 90 °C. The orange form is metastable below 90 °C, and this allows both phases to exist at room temperature. The color variance between phases was shown to arise from a difference in $Cu_2Br_6^{2-}$ chromophore orientation within each phase. The strong pleochroic behavior within each phase was also shown to be a result of this phenomena. The dimer transition was assigned to a p nonbonding ligand to metal charge-transfer transition, and as a result the SPE model was disproved.

Acknowledgment. This research was supported by NSF Grant DMR-8803382. The X-ray diffraction facility was established through funds provided by NSF Grant CHE-8408407 and The Boeing Co. We also thank Mark Shea for performing the powder diffraction experiments.

Supplementary Material Available: Tables of X-ray data collection parameters, atomic coordinates and isotropic thermal parameters, bond angles and distances, anisotropic thermal parameters for non-hydrogen atoms, and hydrogen atom positions and isotropic thermal parameters for both structures (12 pages); observed and calculated structure factor tables for both structures (35 pages). Ordering information is given on any current masthead page.